CASCADES FROM ν_E ABOVE 10^{20} EV

SPENCER R. KLEIN

Nuclear Science Division, Lawrence Berkeley National Laboratory, Berkeley, CA, 94720, USA
E-mail: srklein@lbl.gov

At very high energies, the Landau-Pomeranchuk-Migdal effect reduces the cross sections for electron bremsstrahlung and photon e^+e^- pair production. The fractional electron energy loss and pair production cross sections drop as the energy increases. In contrast, the cross sections for photonuclear interactions grow with energy. In solids and liquids, at energies above 10^{20} eV, photonuclear reactions dominate, and showers that originate as photons or electrons quickly become hadronic showers. These electron-initiated hadronic showers are much shorter (due to the absence of the LPM effect), but wider than purely electromagnetic showers would be. This change in shape alters the spectrum of the electromagnetic and acoustic radiation emitted from the shower. These alterations have important implications for existing and planned searches for radiation from ν_e induced showers above 10^{20} eV, and some existing limits should be reevaluated.

1. Introduction

Although ultra-high energy (UHE) cosmic rays have been studied for many years, their origin is still a mystery. Many cosmic-ray models predict significant fluxes of astrophysical neutrinos with energies above 10^{20} eV. Proposed models consider topological defects, superheavy relics of the big bang[1] and UHE neutrinos as cosmic rays[2]. Conventional approaches predict that the GZK mechanism[3] and gamma ray bursts[4] produce neutrinos with energies above 10^{20} eV.

Several groups have searched for radio or acoustic radiation from electromagnetic cascades produced by interacting ν_e and have reported upper limits on the cosmic flux of ν_e (here, ν_e includes $\overline{\nu_e}$) at energies of 10^{20} to 10^{25} eV. These searches probe enormous volumes to reach interesting upper limits. These limits depend on a good understanding of the cascades that are produced in ν_e interactions.

2. Radio and Acoustic Waves from Showers

Most of the searches have involved radio waves. The Glue collaboration searched for $\approx$ 2.3 GHz radio waves from the moon using two radio-telescopes[5]. FORTE used satellite-based receivers to search for 30-300 MHz radiation from the Greenland ice pack[6]. Both ANITA[7], a balloon-based detector, and RICE[8], a surface antenna array will search for radio waves from ν_e cascades in Antartic ice. The SalSA collaboration plans to search from radio emission from underground salt domes[9].

Translating these search results into a ν_e limit requires a model of the electromagnetic radiation produced by the shower. This radiation has been evaluated using a 3-d Monte Carlo shower simulations[10]. The calculations add the electromagnetic fields from each particle in the shower. This is a computationally demanding process which is only practical for relatively low energy showers, below 1 PeV. At higher energies, extrapolations are used[11,12].

The radiation is large when the electromagnetic fields from the different particles add coherently[13], and the radiated energy is proportional to the square of the shower energy. This happens when the radio wavelength is larger than the transverse spread of the shower, seen along the direction of propagation. The positive and negative charges cancel but, because of positron annihilation, the overall shower contains about 20% more e^- than e^+. This electron excess produces the coherent radiation. When the wavelength is short compared to the lateral size, phase coherence is lost. Radiation from the individual particles adds incoherently, producing a much smaller signal. The degree of coherence depends on the width of the shower; current measurements are largely, but not completely in the coherent domain, so the radiation is sensitive to the transverse shower spreading.

The SAUND collaboration has searched for acoustic radiation from ν_e induced showers, using data from a set of U.S. Navy hydrophones in Bermuda[14]. The acoustic pulse is generated when the electromagnetic cascade heats the water, causing it to expand rapidly around the cascade. The frequencies are low (in the audio range) because the speed of sound is so much lower than that of light. The pulse strength is proportional to the energy deposition. The acoustic frequencies are subject to comparable coherence conditions as the radio studies. The frequency spectrum of the radiation again depends on the shower width.

None of the calculations used in these studies considers the effect of

photonuclear interactions on electromagnetic showers. Here, we show that photonuclear interactions significantly alter ν_e induced showers, and discuss how these interactions affect the shower shape and emitted radiation.

3. Electromagnetic Interactions at High Energies

In high-energy ν_e interactions, the produced electrons receive an average of 80% of the ν_e energy. The remainder is transferred to the target nucleus, producing a hadronic shower.

Electrons with energies $E > 100$ MeV lose energy largely via bremsstrahlung. At somewhat higher energies, electrons lose their energy over a distance scale of order X_0, the radiation length. For ice, $X_0 = 36.1\text{g/cm}^2$. The density of ice depends on its composition (mostly air content). In Antartica, the ice is covered by a layer of compressed snow. For simplicity here, we use a uniform medium with a density of 1 g/cm^2 (as for water), so $X_0 = 36.1$ cm. Almost all ice is within 10% of this value; snow has a somewhat lower density.

At very high energies, the Landau-Pomeranchuk-Migdal (LPM) effect suppresses the bremsstrahlung of low-energy photons, increasing the distance scale. Radiation of photons with energy k from electrons with energy E is suppressed when [15,16]

$$k < \frac{E(E-k)}{E_{LPM}} \tag{1}$$

where E_{LPM} is a material dependent constant,

$$E_{LPM} = \frac{m^4 X_0}{E_s^2} \approx 7.7 \text{ TeV/cm} \cdot X_0. \tag{2}$$

Here m is the mass of the electron, $E_s = m\sqrt{4\pi/\alpha} = 21.2$ MeV, and $\alpha \approx 1/137$ is the fine structure constant. When $E > E_{LPM}$, the effective radiation length $X \approx X_0\sqrt{E/E_{LPM}}$.

Most shower studies calculate LPM suppression using Migdals 1956 calculation of this suppression, albeit with some numerical simplifications[18]. The degree of suppression depends on a variable s

$$s = \sqrt{\frac{E_{LPM}k}{8E(E-k)\xi(s)}}, \tag{3}$$

where $1 < \xi(s) < 2$ increases slowly with s; $s \to \infty$ corresponds to no suppression, while $s \to 0$ gives strong LPM suppression. Figure 1 shows the differential bremsstrahlung cross sections for different electron energies.

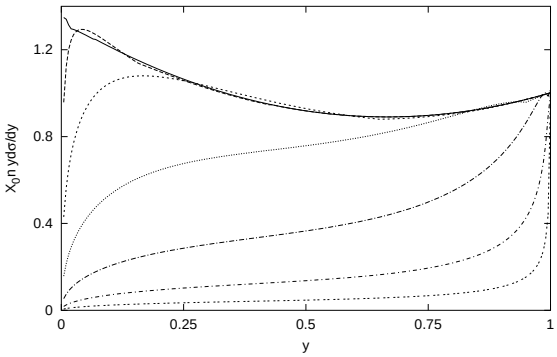

Figure 1. The energy weighted differential cross section per radiation length for bremsstrahlung in water as a function of $y = k/E$ for electrons with energies of 640 GeV (top curve), 6.4 TeV, 64 TeV, 640 TeV, 6.4 PeV, 64 PeV and 640 PeV (bottom curve). These curves apply for other materials for electron energies of 0.0023, 0.023, 0.23, 2.3, 23, 230 and 2300 times E_{LPM}.

Figure 2 compares Migdals calculations with data from SLAC experiment E-146. The figure shows the photon spectrum from 8 and 25 GeV electron beams passing through 3% and 6% X_0 aluminum targets[19]. When $k/E < 10^{-4}$, an additional effect, dielectric suppression, further suppresses bremsstrahlung[20]. At the same time transition radiation from the electron entering and exiting the target increases the photon flux. An experiment at CERN has observed the increase in effective radiation length in bremsstrahlung from 149 to 287 GeV electrons[21].

The cross section for pair production may be similarly reduced; when the photon energy k is greater than E_{LPM}, the pair production cross section is reduced. Figure 3 shows the differential cross section for different photon energies. For a given photon energy, symmetric pairs are suppressed the most.

The reduction in bremsstrahlung cross section corresponds to a reduction in energy loss (dE/dx) by the electron. Fig. 4 shows the reduction in bremsstrahlung dE/dx as a function of incident electron energy. Also shown is the reduction in pair production cross section, as a function of photon energy. Photons are affected by LPM suppression at much higher energies than electrons.

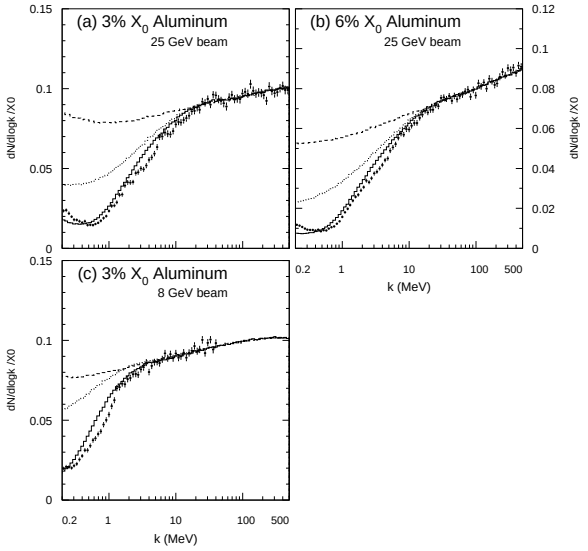

Figure 2. Data (points) from 8 and 25 GeV electrons passing through aluminum targets, from the SLAC E-146 collaboration, compared with calculations based on the Bethe-Heitler (dashed histogram), and Migdals LPM suppression (dot-dashed histogram), and on Migdals calculations with LPM and dielectric suppression (solid histogram). The data is binned logarithmically in photon energy, so the Bethe-Heitler $1/k$ spectrum is roughly flat.

4. Photonuclear Interactions

In contrast to pair production, for $k > 10$ TeV, the cross section for photonuclear interactions increases with energy[22]. The dominant contribution to the photonuclear cross section (from 'soft' interactions) can be described in terms of photon-Pomeron interactions. The cross section for photon-proton interactions rises with the γp center of mass energy W as $W^{0.16}$. At very high energies, the photon may also interact directly with a quark in the target, $\gamma q \to gq$. Data from HERA on γp interactions extends up to $W = 200$ GeV[30], equivalent to 20 TeV photons striking stationary protons. Direct γq interactions have not clearly been observed at HERA, so predictions about this process have significant uncertainties.

For oxygen, a Glauber calculation accounts for interactions with multiple nucleons (shadowing). This moderates the W-dependence of the cross section. Since oxygen has only 16 nucleons, the number of multiple interactions is fairly small. Here, we assume that the effect of shadowing in

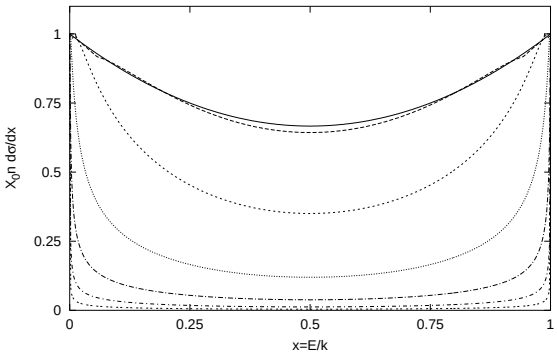

Figure 3. The differential cross section for pair production in water, as a function of $x = E/k$ for photons with energies of 64 TeV (top curve), 640 TeV, 6.4 PeV, 64 PeV, 6400 PeV, 6.4 EeV and 64 EeV (bottom curve). These curves apply for other materials for photon energies of 0.23, 2.3, 23, 230, 2300, 23,000 and 230,000 E_{LPM}.

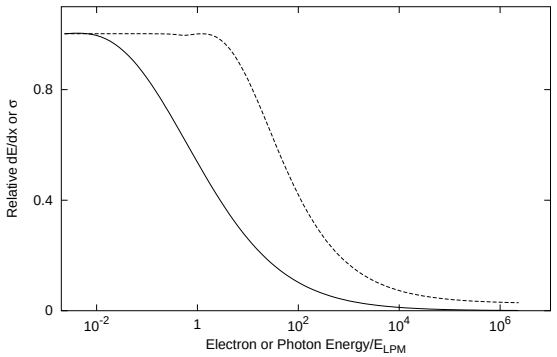

Figure 4. The electron energy loss (dE/dx) for electron bremsstrahlung (solid line) and the photon pair conversion cross section (solid line), relative to the Bethe-Heitler predictions (*i.e.* with no LPM suppression) as a function of E/E_{LPM}.

oxygen and direct photon interactions in oxygen and hydrogen cancel each other out, so the photon-H_2O cross section follows the Pomeron trajectory, $\sigma \approx W^{0.16}$. This leads to a lower total cross section than in the original model[22], and a slightly higher crossover energy than is given in Ref. [23]. For water, this is a reasonable approximation, but, for heavy nuclei, it may somewhat underestimate the shadowing and overestimate the cross-section.

Figure 4 compares these photonuclear cross sections with the pair production cross section in lead and water. In both materials, photonuclear interactions dominate for $k > 10^{20}$ eV. The cross-over energy is similar

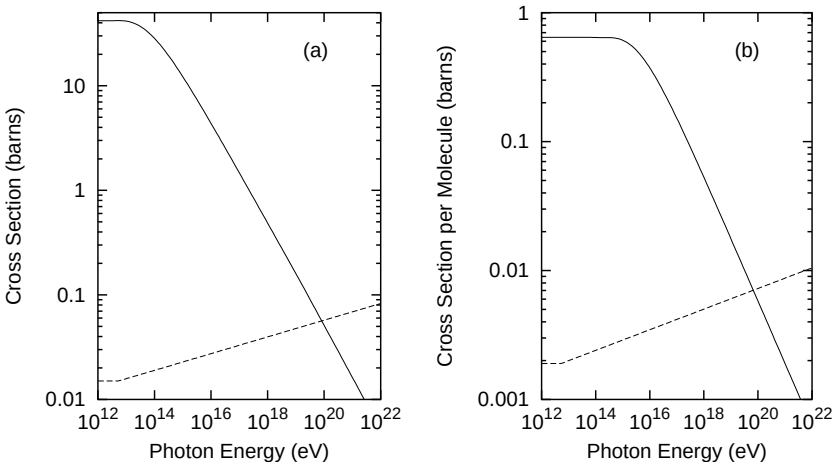

Figure 5. Comparison between the pair production and photonuclear interaction cross sections in (a) lead and (b) water. Above an energy of 10^{20} eV, the photonuclear cross section is larger than for pair production.

for diverse solids and liquids because the increase in $\sigma_{\gamma p}/\sigma_{ee}$ for heavier nuclei is cancelled out by the decrease in E_{LPM} as X_0 drops. Lunar soil has a density of 1.7 g/cm[25], and should have a similar crossover energy. In gasses, because of the reduced density, but similar atomic number, the crossover point occurs at much higher energies (about 5×10^{22} eV in air at sea level).

5. Shower Length

A ν_e interaction produces a high-energy electron plus a hadronic shower from the struck hadron. Because of the LPM effect, an energetic electron will travel a long distance before losing its energy. Figure 4 shows that the electron interaction distance can be approximated

$$X_e(E) = X_0 \sqrt{\frac{2E}{E_{LPM}}} \tag{4}$$

for $E > E_{LPM}$. Here, we neglect electro-nuclear interactions and direct pair production. At sufficiently high energies, these processes will be the dominant energy loss mechanisms, and electrons will act like muons[24]. However, these ultra-high energy electron interactions have not yet been studied in detail, and so we neglect them here.

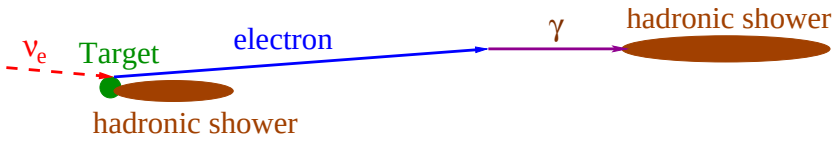

Figure 6. Diagram of UHE ν_e shower development with photonuclear interactions (not to scale).

When the LPM effect is strong (*i.e.* above 10^{20} eV), the electron transfers most of its energy to a single photon. For photon energy $k \gg E_{LPM}$, the photon pair production distance is

$$X_\gamma(k) = X_0\sqrt{\frac{k}{50E_{LPM}}}, \tag{5}$$

10 times shorter than X_e at the same energy. When the pair production cross section falls below the photonuclear cross section, the photon will usually interact hadronically. The hadronic interaction length is $1/\sigma\rho$, where σ is the photonuclear cross section per molecule (from Fig 4), and ρ is the target density. In water, $\rho = 3.3\times10^{22}$ molecules/cm^3, and, at 10^{20} eV, the hadronic interaction length in is about 43 m. Figure 6 shows schematically how showers evolve with photonuclear interactions.

We will use a simple model to compare the development of ν_e cascades with and without photonuclear interactions. Although inaccurate, these models are useful for comparison. Purely electromagnetic showers evolve via bremsstrahlung and pair production, with each succeeding shower generation containing twice as many particles as the last, each with half of the energy. Shower development continues until the average particle energy drops below the critical energy, E_c. Below this energy, Compton scattering becomes more important than bremsstrahlung and the shower quickly dissipates its energy into the medium. This occurs after $N = \ln_2(E/E_c)$ generations. In water, $E_c = 126$ MeV, so for $E = 10^{20}$ eV, $N = 40$. Without the LPM effect, a generation occurs in 1 X_0, which is 36.1 cm in water. The shower length is $40X_0 \approx 15$ m. Some authors[10,25] have used $X_0 \ln 2$ for the generation length; this leads to showers that are 30% shorter than are given here.

The LPM effect does not affect the number of generations. However, the effective radiation length increases rapidly. When the LPM effect is large, the effective radiation length for a generation with average particle

energy E_g is roughly

$$X = X_0\sqrt{\frac{E_g}{5E_{LPM}}}. \quad (6)$$

This length is the geometric average of $X_e(E)$ and $X_\gamma(k)$ For each successive generation, X decreases by $1/\sqrt{2}$.

Figure 7 shows the ν_e shower length as a function of energy. For purely electromagnetic showers, above 10^{18} eV, the LPM effect reduces the cross sections and the length increases rapidly. This length increase has been experimentally observed[26]. The LPM effect also increases the shower-to-shower variation[27], complicating measurements.

Alvarez-Muniz and Zas also studied the length of electromagnetic showers[11]. They defined the length as the distance over which the shower has more than a given fraction (10%, 50% or 70%) of the maximum number of particles. Above 10^{16} eV, where the LPM effect is significant, their length scales as $E^{1/3}$. For the 70% fraction, their lengths are slightly larger than are given here: 6 m vs. 4.8 m at 1 TeV, and 37 m vs. 20 m at 10^{18} eV. With a slightly lower containment fraction, the curves would probably agree fairly well.

For hadronic showers, there are no simple parameterizations. Because of the higher final state multiplicity (compared to e^+e^- pairs) and the absence of LPM suppression, hadronic showers develop more rapidly than electromagnetic showers with similar energies. Here, we use a simple model which generously overestimates the penetration of hadronic showers: we treat them as electromagnetic showers, with each generation having only twice as many particles as the previous one. Each generation develops over a distance Λ, the hadronic interaction length; $\Lambda = 83$ cm in water. This parameterization is shown by the dotted line in Fig. 7. For the energies for which data is available[28], this thickness is more than enough for 99% containment of hadronic showers. At high energies, this parameterization might overestimate the shower length by 30-70%. Still, at 10^{20} eV, the shower is 3 times shorter than an electromagnetic shower; by 10^{23} eV, the difference is a factor of 100.

In solids, high-energy π^0 (and some η) interact before they can decay. This happens when the decay length, $\gamma\beta c\tau$ is larger than Λ. In water, $\gamma\beta c\tau > \Lambda$ when $E_\pi > 5$ PeV. For the η, interactions predominate for $E_\eta > 3$ EeV. So, a 10^{20} eV hadronic shower develops through several generations before a significant electromagnetic component develops. The electromagnetic particle energies will be low enough that the LPM effect will be absent.

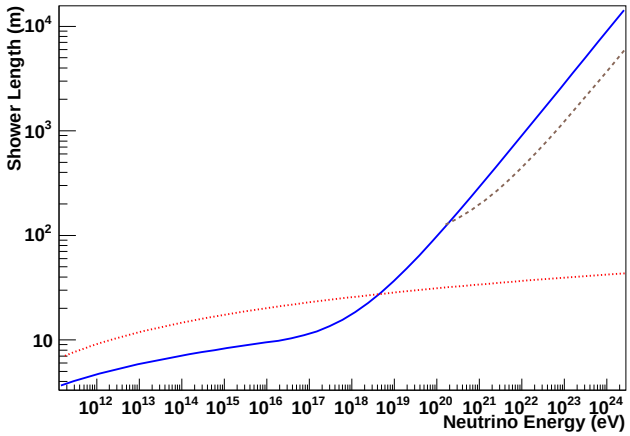

Figure 7. Shower length as a function of neutrino energy. The solid blue line is for a purely electromagnetic shower, while the dashed brown line is for a hybrid EM/hadronic shower. The dotted red line is for a purely hadronic shower. The difference between the hybrid and purely hadronic showers is that the hybrid includes the long electron path before bremsstrahlung, and the photon path before it interacts hadronically. For the hybrid and electromagnetic showers, the electron is assumed to take 80% of the ν_e energy.

Simulations confirm that the LPM effect only occasionally affects hadronic showers, when a high energy π^0 or η decays[29].

The dashed brown line in Fig. 7 shows the typical length of hybrid ν_e showers that develop as shown in Fig 6. In F.g 7, electrons take 80% of the neutrino energy and photons take 90% of the electron energies. As Fig. 1 shows, this is a reasonable energy partition.

Hybrid showers are much longer than purely hadronic showers because of the length of the electron and photon tracks. Above an energy of 10^{20} eV, hybrid showers are much shorter than purely electromagnetic showers. The presence of photonuclear reactions greatly shortens the ν_e showers.

Much of the length comes from the initial electron trajectory. In both treatments, electron energy loss due to direct pair production and electronuclear interactions is neglect. With a realistic treatment of these effects, both electromagnetic and hybrid showers would become shorter, and the fractional difference would increase.

Above 10^{23} eV, the hybrid shower length exceeds 1 km, comparable to the typical thickness of the ice or water used for neutrino detection. Even

if a vertically downward-going neutrino interacts near the target surface, the bulk of the signal (which comes from the end of the shower, when the number of particles is largest) will be induced in the rock underneath the sensitive medium, limiting the sensitivity to near-vertical showers; this may be particularly relevant for SAUND. Above 1 PeV, the earth is opaque to neutrinos, so there are no corresponding upward-going neutrinos.

Some analyses avoid the shower-length problem by considering only radiation from hadronic cascades from struck nuclei[6]. Analyses that include emission from the 2nd, photon-produced hadronic cascades may find lower limits and/or energy thresholds.

6. Shower Lateral Distributions

The characteristic lateral spread of electromagnetic shower is given by the Moliere radius, $r_M = X_0 E_s/E_c = 6.2$ cm in water[30]. For hadronic showers, there is no corresponding simple formula for lateral distributions.

To compare the widths of electromagnetic and hadronic showers in solids (liquids should be similar), we consider data from the CERN LAA project[31]. The collaboration compared the lateral distributions of 5- 150 GeV electromagnetic and hadronic showers in a lead/scintillating fiber calorimeter. The showers were produced by electron and π^- interactions respectively. They modelled the electromagnetic lateral energy density as

$$\frac{dE}{dA} = \frac{A}{r}\frac{1}{(r^2+B^2)^2} \tag{7}$$

where A is the size of the signal, and B is the shower width. They found $B \approx 2$ cm, almost independent of energy. They parameterized the lateral distribution of hadronic showers with 2 components:

$$\frac{dE}{dA} = \frac{B_1}{r}e^{-r/\lambda_1} + \frac{B_2}{r}e^{-r^2/\lambda_2^2}. \tag{8}$$

where B_1 and B_2 are the sizes of the two components and λ_1 and λ_2 are the lateral spreads of the two components. Neither λ_1, λ_2 nor B_2/B_1 varied significantly with energy.

Figure 8 compares these energy depositions (in terms of charge Q deposited in the calorimeter as a function of radius, dQ/dr), for 150 GeV electromagnetic and hadronic showers. For electromagnetic showers, half of the energy is deposited within a cylinder of 0.9 cm radius; for hadronic showers, 2.8 cm is required for the same containment. For 80% containment radii of 1.9 cm and 11 cm are required for electromagnetic and hadronic showers, respectively. For 90% containment, the radii are 2.8 cm and 21 cm.

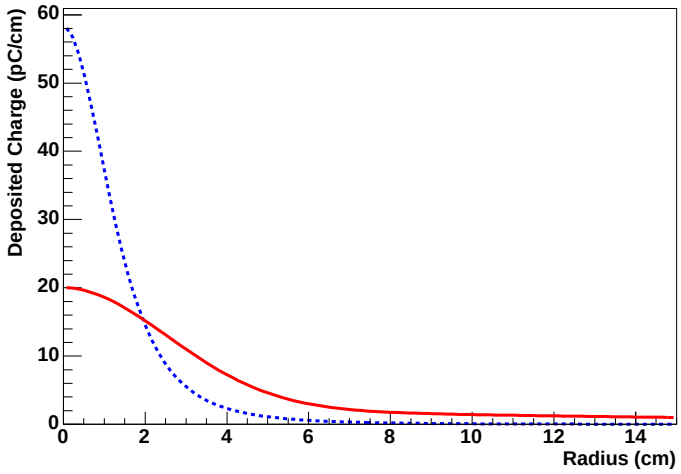

Figure 8. Lateral profiles of charge deposition dQ/dR for 150 GeV electromagnetic (dashed line) and hadronic (solid line) showers as observed by the LAA project.

Depending on the containment criteria, the hadronic showers have radii 3 to 8 times larger than electromagnetic showers.

The CERN LAA calorimeter showers developed largely in lead; water has much lighter nuclei. However, the lateral spread of the shower depends on the transverse momentum of the particles produced in the interactions; the p_T distributions should be very similar for lead and water.

In very high energies hadronic interactions, hard parton-parton interactions will dominate the cross section. Scattered high transverse momentum (p_T) partons will fragment into high p_T hadrons[32]. At high collision energies, these high p_T hadrons will widen the hadronic showers. We do not estimate the magnitude of the increased broadening here, but it could be substantial.

In contrast, the transverse momentum of electromagnetic showers comes largely from multiple scattering. The p_T from multiple scattering is independent of energy. A small fraction of the p_T does come from the pair production and bremsstrahlung reactions themselves. When LPM suppression is large, the mean opening angle (and, hence, p_T) in bremsstrahlung and pair production increase by a factor S, the suppression factor for the angle-independent calculation[16,33]. However, because multiple scattering contributes most of the p_T, the shower width is not significantly affected.

Because of the hadronic broadening with increasing collision energy,

the width ratios measured at 150 GeV should be treated as lower bounds at 10^{20} eV. Detailed simulations are needed to develop a better estimate. Even though the low-energy part of the shower is largely electromagnetic, it retains the lateral spread acquired during it's high-energy hadronic evolution; the CERN LAA measurements were sensitive to both the hadronic and electromagnetic components of the showers.

7. Electromagnetic Radiation from Showers

Coherent radio Cherenkov emission is dominated by the low-energy part of the shower, where the net charge excess of e^- over e^+ leads to significant radiation[34]. The frequency spectrum of the radiation depends on the width of the shower. An accurate calculation of the frequency spectrum requires a full simulation and a detailed calculation. Here, we will consider some simple models which should qualitatively illustrate the features which may be expected from a full calculation.

Coherent Cherenkov radio emission occurs when the radio wavelength is larger than the shower width; if the wavelength is small compared to the width, coherence is lost. Alvarez-Muniz and Zas studied the effect of lateral spreading by comparing the radiation from a full 3-dimensional electromagnetic cascade calculation of a 10 TeV shower with a simplified 1-dimensional calculation[12]. The importance of the lateral spread depends on the observation angle. Coherence is maximal when the observer looks along the Cherenkov angle, $\theta_C = 56^0$ in ice (and a similar value in the lunar regolith[5]). For frequencies above $\approx$ 500 MHz, Alvarez-Muniz and Zas found that the lateral spread significantly reduces the radiation. This is within the frequency range explored by most of current experiments; these experiments are sensitive to the lateral spreading.

An observer looking at the Cherenkov angle θ_C sees an apparent shower thickness given by the lateral spread times $1/\sin(\theta_C)$ (about 1.21 in water). In hybrid showers, the apparent thickness may be several times higher than in purely electromagnetic showers; a the lateral spread due to the hadronic interactions could have an important effect at frequencies as low as 60-200 MHz. At higher frequencies, there will be a significant loss of coherence, and the radiation will be reduced.

Buniy and Ralston[35] found that the radiation from a shower can be found using the Fourier transform of the charge distribution. They worked in the low frequency limit, where the lateral spread of the form factor had no effect. This approximation fails at high frequencies. The region of validity

is much smaller for hybrid showers than for purely electromagnetic ones.

The acoustic radiation from a shower comes from what is effectively a line source which radiates largely perpendicular to the shower direction; the shower looks like an expanding pancake. The acoustic frequency spectrum depends on the lateral spread of the shower. For a speed of sound of 1500 m/s[36], the maximum frequency for full coherence (i.e. the shower is contained within one acoustic wavelength) drops from 75 kHz to 12.5 kHz when going from electromagnetic to hybrid showers (for 80% lateral containment). This covers most of the frequency range studied by SAUND.

8. Other Implications

Although photonuclear interactions only dominate above 10^{20} eV, they may affect showers at considerably lower energies, by introducing hadronic components into largely electromagnetic showers. This could affect searches for 10^{18} eV neutrinos produced by cosmic ray interactions with the cosmic microwave background[37].

At intermediate energies (10^{16} - 10^{20} eV), photonuclear interactions convert some electromagnetic shower energy into hadrons. For example, a 10^{19} eV shower evolves through stages that include ≈ 10 10^{18} eV particles and ≈ 100 10^{17} eV particles, half photons and half electrons. At 10^{18} and 10^{17} eV, the probabilities for photonuclear interactions are about 12% and 3% respectively. These probabilities are high enough that most showers with energies above 2×10^{18} eV will have some hadronic component. The produced hadrons may decay and introduce a muon content into the shower. Although most $\pi^{\pm}$ and kaons interact before they can decay, charm and bottom hadrons produced in the shower may decay semi-leptonically, producing muons. These muon 'tails' could be used to provide ν_e directional information in experiments like IceCube[38].

The initial hadronic shower from the ν_e interaction, plus the delayed hadronic shower after the electron to photon to hadronic shower conversion could mimic a ν_τ 'double-bang' event[39]. The electron plus photon range equals $\gamma\beta c\tau$ for a τ ($c\tau = 290$ fs) at a neutrino energy around 1 PeV. The probability of photonuclear interactions at this energy is small. However, there are large fluctuations in τ decay length, in energy division (between the lepton and the target nucleon) and measurement, and in shower development; all of these may increase the likelihood of misreconstruction and consequent misidentification. An accurate estimate of the misidentification probability requires detailed simulations.

9. Uncertainties

There are significant uncertainties in these calculations. There are approximations in Migdals calculations and uncertainties in the additional suppression mechanisms and the photonuclear calculations.

Migdals calculations do a good job of describing the SLAC E-146 and CERN data, with the apparent exception of the E-146 data on carbon targets[19]. Nevertheless, they have some limitations. Migdal assumed that the scattering was Gaussian; A Gaussian distribution considerably underestimates the number of large-angle Coulomb scatters, and could therefore, under-estimate the suppression. Migdal neglected interactions with the atomic electrons in the target. This may be important for low-Z targets.

Two newer and more sophisticated calculations, by Zakharov[40] and by Baier and Katkov[41], remedy these problems. Both include accurate models of Coulomb scattering and account for atomic electrons by using separate elastic and inelastic potentials. Both calculations match the experimental data. Unfortunately, code for these calculations is not publicly available for use in simulations. However, Baier and Katkov give a cross section for high-energy ($k \gg E_{LPM}$) pair conversion which agrees with Migdals calculation to within about 20%, well within the accuracy needed here.

None of these calculations explicitly consider hydrogen targets. Hydrogen is problematic because the standard Thomas-Fermi screening calculations are only accurate for atomic numbers $Z > 5$. A hydrogen-specific screening correction is required to accurately find the cross sections[42]. However, because pair production in water is dominated by interactions with oxygen, the error in the hydrogen screening causes much less than a 10% effect on the cross sections for water.

Other suppression mechanisms may enter at very high energies. When the formation length (reaction zone) is long enough, a nascent photon may interact, by either pair production or photonuclear interactions) before it is fully formed. Bremsstrahlung and pair production may suppress each other, and photonuclear interactions may suppress bremsstrahlung. These effects may be important when the formation length (including the LPM effect) is larger than X_0 or $1/\sigma\rho$. The former can only occur when $E > E_p$, where $E_p = 540$ TeV in water[16]. At this energy, it only applies for a very narrow range of k/E (or, for photons, E/k). The range of k/E (or E/k) where it applies is only significant at much higher energies; above 10^{20} eV. However, this mechanism won't change the conclusion that photonuclear reactions dominate above 10^{20} eV. If anything, the mutual suppression further re-

duces the electromagnetic cross sections, strengthening this conclusion.

A broader question for all of the electromagnetic interactions involves higher-order reactions like $eN \rightarrow e^+e^-eN$ (direct pair production) and $\gamma N \rightarrow e^+e^-\gamma$[16]. Normally, the cross section for these higher order reactions are a factor of order $\alpha = 1/137$ smaller than the leading-order processes. However, the higher-order processes require a higher momentum transfer from the target, and so are much less subject to LPM suppression. When LPM suppression is large, these higher-order reactions could dominate, creating a floor for the electromagnetic cross sections. Detailed comparisons have not been done, but 1/137 suppression is only reached at energies above 10^{20} eV.

The final caveat involves photonuclear interactions. The extrapolation to 10^{20} eV is a factor of 2000 in W beyond the HERA data. Between the possible moderation of the $W^{0.16}$ Pomeron trajectory and uncertainties in direct γq cross sections, the uncertainties are considerable. However, because of the slow energy variation, the large extrapolation uncertainty cannot radically change the crossover energy. Even a 50% reduction in the rise in cross section above the HERA data (i.e. for $k > 20$ TeV) would only increase the crossover energy by about 40%.

In short, although there are significant uncertainties present, even generous error estimates do not affect the conclusion that photonuclear cross sections are larger than electromagnetic ones for ν_e energies above 10^{20} eV.

10. Conclusions

At energies above 10^{20} eV, photons are more likely to interact hadronically than through pair production, and ν_e showers are likely to be hadronic. By 10^{21} eV, hadronic showers are 4 times as frequent as electromagnetic showers. These hadronic showers are considerably shorter, and several times wider than purely electromagnetic showers. The increased width of the showers reduces the frequencies at which radio and acoustic radiation are coherently emitted, and may affect the conclusions of experiments that study radio and/or acoustic emission from ν_e showers.

It is a pleasure to acknowledge useful discussions about photonuclear interactions with Ralph Engel and Mark Strikman. Dmitri Chirkin and Bob Stokstad made useful comments about this manuscript. It is also a pleasure to thank the UCB and LBNL IceCube groups for many useful pointers. I also thank the workshop organizers for putting together a very interesting week. This work was funded by the U.S. National Science Foundation

under Grant number OPP-0236449 and the U.S. Department of Energy under contract number DE-AC-76SF00098.

References

1. G. Gelmini and A. Kusenko, Phys. Rev. Lett. **84**, 1378 (2000); P. Bhattacharjee and G. Sigl, Phys. Rept. **327**, 109 (2000).
2. D. Fargion *et al.*, astro-ph/0303233 and references therein; Z. Fodor, S. D. Katz and A. Ringwald, JHEP **0206**, 46 (2002); S. Yoshida, G. Sigl and S. Lee, Phys. Rev. Lett. **81**, 5505 (1998).
3. C. Lauchard *et al.*, Nucl. Phys. Proc. Suppl. **110**, 525 (2002); D. Fargion and B. Mele, astro-ph/9906451.
4. E. Waxman and J. Bahcall, Phys. Rev. Lett. **78**, 2292 (1997).
5. P. Gorham *et al.*, Phys. Rev. Lett. **93**, 041101 (2004).
6. N. G. Lehtinen *et al.*, Phys. Rev. **D69**, 013008 (2004).
7. A. Silvestri *et al.*, astro-ph/0411007.
8. I. Kravchenko *et al.*, astro-ph/0306408; I. Kravchenko *et al.*, Astropart. Phys. **20**, 195 (2003).
9. P. Gorham *et al.*, Nucl. Instrum. & Meth. **A490**, 476 (2002).
10. E. Zas, F. Halzen and T. Stanev, Phys. Rev. **D45**, 362 (1991).
11. J. Alvarez-Muniz and E. Zas, Phys. Lett. **B411**, 218 (1997).
12. J. Alvarez-Muniz, R. A. Vasquez and E. Zas, Phys. Rev. **D62**, 063001 (2000).
13. G. A. Askaryan and B. A. Dolgoshein, JETP Lett. **25**, 213 (1977).
14. J. Vandenbroucke, G. Gratta and N. Lehtinen, astro-ph/0406105.
15. L.D. Landau and I. J. Pomeranchuk, Dokl. Akad. Nauk SSR **92**, 535 (1953); L.D. Landau and I. J. Pomeranchuk, Dokl. Akad. Nauk SSR **92**, 735 (1953).
16. S. Klein, Rev. Mod. Phys. **71**, 1501 (1999).
17. A. B. Migdal, Phys. Rev. **103**, 1811 (1956).
18. T. Stanev *et al.*, Phys. Rev. **D25**, 1291 (1982).
19. P. Anthony *et al.*, Phys. Rev. Lett. **75**, 1949 (1995); P. Anthony *et al.*, Phys. Rev. **D56**, 1373 (1997).
20. P. Anthony *et al.*, Phys. Rev. Lett. **76**, 3550 (1996).
21. H. D. Hansen *et al.*, Phys. Rev. **D69**, 032001 (2004); H. D. Hansen *et al.*, Phys. Rev. Lett. **91**, 014801 (2003).
22. R. Engel, J. Ranft and S. Roessler, Phys. Rev. **D55**, 6957 (1997).
23. S. Klein, hep-ex/0402028.
24. D. Chirkin and W. Rhode, hep-ph/0407075.
25. W. Heitler, *The Quantum Theory of Radiation*, 3rd edition, Oxford, 1954.
26. K. Kasahara, Phys. Rev. **D31**, 2737 (1985).
27. S. Klein, astro-ph/9712198.
28. R. Wigmans, *Calorimetry Energy Measurement in Particle Physics*, Clarendon Press, 2000.
29. J. Alvarez-Muniz and E. Zas, Phys. Lett. **B434**, 396 (1998).
30. S. Eidelman *et al.*, Phys. Lett. B**592**, 1 (2004).
31. D. Acosta *et al.*, Nucl. Instrum. & Meth. **A316**, 184 (1992).
32. G. Sterman *et al.*, Rev. Mod. Phys. **67**, 157 (1995).

33. V. M. Galitsky and I. I.Gurevich, Nuovo Cimento, **32**, 396 (1964).
34. D. Saltzberg *et al.*, Phys. Rev. Lett. **86**, 2802 (2001).
35. R. V. Buniy and J. P. Ralston, Phys. Rev. **D65**, 016003 (2002).
36. N. G. Lehtinen *et al.*, Astropart. Phys. **17**, 279 (2002).
37. J. Alvarez-Muniz and F. Halzen, astro-ph/0102106.
38. F. Halzen, astro-ph/0311004.
39. J. Learned and S. Pakvasa, Astropart. Phys. **3**, 267 (1995).
40. B. G. Zakharov, Yad. Fiz. **61**, 924 (1998).
41. V. N. Baier and V. M. Katkov, Phys. Rev. **D62**, 036008 (2000).
42. Y.S. Tsai, Rev. Mod. Phys. **46**, 815 (1974).